On Multifrequency Strategies of Use of G.P.R. Systems.

Raffaele Persico, Giovanni Alberti, Salvatore Esposito
CO.RI.S.T.A. - Consortium for Research on Advanced Remote Sensing Systems
Piazzale Tecchio 80, 80125 Napoli, Italy

Giovanni Leone
Dipartimento di Informatica, Matematica, Elettronica e Trasporti, Università di Reggio Calabria
Via Graziella, 89100, Reggio Calabria, Italy

Francesco Soldovieri
Dipartimento di Ingegneria dell'Informazione, Seconda Università degli Studi di Napoli
Via Roma 29, 81031, Aversa (CE), Italy

ABSTRACT

In the framework of ARCHEO, a national research project funded by the Italian Ministry for Universities and Scientific and Technological Research (M.U.R.S.T.), a new ground penetrating radar (GPR) has been developed by the Italian Consortium for Research on Advanced Remote Sensing Systems (CO.RI.S.T.A.). The system has been specially designed to meet archaeological requirements and it will be tested the two archaeological sites of Sinuessa and Cales, in the Southern Italy.

An innovative feature of ARCHEO concerns the exploitation of a that a multiview multistatic measurement scheme (at several frequencies) rather than a more common multimonostatic (or multibistatic).

In order to reconstruct buried objects starting from the measurement data collected with such an acquisition strategy, it is made use of an inverse scattering technique.

With the real project ARCHEO in mind (in particular this scheme of measurement), this paper deals with a theoretical discussion on the features of the class of retrievable profiles by G.P.R. data, within the framework of a linear model for electromagnetic scattering in a two dimensional lossless half space. For a given range of frequencies exploitable, multiview multistatic measurements can be useful in G.P.R. prospecting because they can provide information on low spatial harmonic components of an unknown object not attainable from the a multimonostatic scheme exploiting the same frequency range.

In particular, we show that, for a given band of work frequencies, the class of the unknowns retrievable by a multiview multistatic multifrequency measurement configuration can be is not much different from that attainable within a multimonostatic configuration with the addition of multiview multistatic data taken at the lowest of the frequencies adopted.

Keywords: multiview, multistatic, multifrequency, multimonostatic.

1. INTRODUCTION

The first ideas of investigating subsoil properties by electromagnetic waves, by this time have been drawn up almost a hundred years ago[1], and in this century an endless set of applications has been progressively contrived, so that nowadays GPR are exploited to detect mines, to retrieve archaeological finds, to discover buried objects within policy inquiries etc[2]. This has required a refinement of both the technologies and the processing techniques of GPR data. In particular, the introduction –in the seventies- of the stepped frequency ground penetrating radar (SFGPR)[3], in addition to several technological advantages and to the possibility to achieve a higher signal to noise ratio[3-4], maybe has made it easier to think of processing GPR data in the frequency domain rather than in time domain. In particular, the SFGPR was conceived as a tool to synthesize equivalent pulses in time domain by acting in the frequency domain[4-6]. So, it is commonly used within a "radar" approach where the detection of the buried objects is performed by means of the reflected "echoes". However, in the last years the SFGPR has been interpreted also as a tool for a "tomographic" approach to the reconstruction of the dielectric properties of the buried objects. This approach is based on considering the mathematical relationship that links them to each other[7]. In other words, it is possible, within certain limits, to invert this mathematical relationship rather than to limit oneself

Image Reconstruction from Incomplete Data, Michael A. Fiddy, Rick P. Millane, Editors,
Proceedings of SPIE Vol. 4123 (2000) © 2000 SPIE. · 0277-786X/00/$15.00

to the detection of echoes from buried bodies, and this can be done under the framework of various models[7-9] for the electromagnetic scattering. In this work we refer to the linear (distorted) Born model[10], well known from literature[7-18]. The relationship quoted above depends, among other things, on the configuration of the measurements, i.e. the number of retrievable unknowns and the class of retrievable objects depend on the way in which the measurements are arranged. In particular, we are concerned with the investigation of non-redundant configurations, i.e. measure configurations which allow to gather as much as possible of the information about the unknown permittivity profile for a given number of measurements. This paper is meant to analyze a multiview multistatic and multifrequency[11, 18] configuration and to compare it with a multimonostatic[1, 11-13] configuration with the addition of multistatic multiview[7-9, 11, 14-17] data collected at the lowest exploited frequency. The purpose of this work is to point out that the two configurations provide "similar" results, even if the second one needs in general a much lower number of measurements. The analysis is performed in a lossless two dimensional half space. Numerical examples are provided to confirm the mathematical previsions exposed in next section. It is to be outlined that a multistatic multiview configuration of measurements requires a positioning system of the antennas to move them independently of each other and in a controlled way, whereas the more "classical" multimonostatic configuration does not need any positioning system, because the transmitting and the receiving antennas are mechanically linked to each other and cannot move independently. Therefore, in order to exploit the capabilities (analyzed in the following) of a multiview multistatic scheme, within the project ARCHEO a positioning system has been also designed[19].

The work is organized as follows: in next section the formulation of the problem is given within the linear Born distorted model, in section 3 numerical examples are shown and conclusions follow in section 4.

2. FORMULATION OF THE PROBLEM

The geometry of the problem is depicted in fig. 1. The source of field is a filamentary current at the abscissa x_s, variable along the line Σ at quote h=0. The field scattered by two dimensional buried objects inside the buried probed region D is measured at the observation abscissa x_o variable along Σ too. The current is time harmonic, and the band of work frequencies is a fixed finite interval (f_{min}, f_{max}).

In this section two acquisition strategies are compared in order to determine the class of retrievable unknowns. The first one is a multiview multistatic multifrequency configuration (i.e. a configuration obtained by varying x_s and x_o independently on each other and by also switching "freely" the frequency between f_{min} and f_{max}), that from now on will be called "the configuration 1" for sake of simplicity.

The second one is a multimonostatic configuration (i.e. measurement are obtained by fixing $x_s=x_o$ and by varying x_o along Σ and f over $[f_{min}, f_{max}]$) with the addition of the data taken by a multiview multistatic configuration at frequency $f=f_{min}$. From now on this configuration of measure will be called "the configuration 2".

In the following k_s, k_{smin} and k_{smax} will indicate respectively the wavenumber of the soil at a fixed frequency f, the wavenumber of the soil at $f=f_{min}$ and the wavenumber of the soil at $f= f_{max}$. Moreover k_o will indicate the wavenumber of the air (considered equal to the free space) at a given frequency f. Let us recall that we refer to a formulation of the problem within the framework of the distorted Born model[10] adopted in refs. 7, 11-13, 15.

The unknown function is the difference of relative dielectric permittivity $\Delta\varepsilon_r$ between the object and the surrounding soil within the probed region D, i.e. the quantity:

$$\Delta\varepsilon_r \equiv \frac{\varepsilon_{ob}(\vec{r}) - \varepsilon_s}{\varepsilon_o} \tag{1}$$

where $\varepsilon_{ob}(\vec{r})$ is the unknown absolute permittivity profile as a function of the position vector variable in D, and where ε_s and ε_o are respectively the (constant) absolute permittivities of the soil and of the free space.

As shown in Appendix A, under the Born Distorted Approximation the linear integral relationship between $\Delta\varepsilon_r$ and the scattered field, at a fixed frequency f is given by:

$$E_s(x_s,x_o)=j2\pi f I_o\mu_o\left\{\frac{1}{4\pi^2}\int_{-\infty}^{+\infty}\int_{-\infty}^{+\infty}\frac{\exp[jv(x_s)]\exp[ju(x_o)]}{[w_o(v)+w_s(v)][w_o(u)+w_s(u)]}\times\right.$$
$$\left.\left[\int_0^{+\infty}\exp[-j(w_s(u)+w_s(v))z']dz'\int_{-\infty}^{+\infty}\Delta\varepsilon_r(x',z')\exp(-j(u+v)x')dx'\right]dudv\right\} \quad (2)$$

where E_s is the scattered field, $w_o(u)=\sqrt{k_o^2-u^2}$ and $w_s(u)=\sqrt{k_s^2-u^2}$ (the imaginary part of the square root is to be taken not positive) and I_o is the current level. Eq. 2 points out the dependence of the scattered field on the source and on the observation point.

A theoretical comparison is provided by exploiting the fact that the data allow to retrieve the Fourier transform of the unknown object in a finite region, as shown in Appendix A for a multiview multistatic case and in appendix B for a multimonostatic case. This implies that also the configurations 1 and two allows to retrieve the spectrum of the unknown profile in a finite region. The finite region wherein the configuration 1 makes possible the reconstruction of the spectrum of the object is depicted in fig. 2 and it is the comprehensive spectral set Ω given by the union of the lower set Ω_l and of the upper annulus Ω_m also depicted in fig. 2, wherein η denotes the conjugate variable of the horizontal direction x and ζ denotes the conjugate variable of the depth z (all calculations are exposed in Appendix A). The set Ω is delimited by the η-axis and by three half-circles whose equations are respectively: $\eta^2+\zeta^2=4k^2_{smax}$, $(\eta-k_{smin})^2+\zeta^2=k^2_{smin}$, $(\eta+k_{smin})^2+\zeta^2=k^2_{smin}$. The class of retrievable functions is expected to be strongly related to this spectral set (see ref. 8 and ref. 11 for a deeper analysis in a one dimensional case). Therefore, if another measurement configuration provided the spectrum of the unknown dielectric profile in the same spectral set, it would be expected to allow the retrieving of a similar class of objects. The point of this paper is exactly this: the configuration 2 allows, in a certain sense, to cover the same spectral set Ω. Precisely, based on the calculations of Appendix A, the multiview multistatic configuration at frequency f_{min} allows to retrieve the spectrum of the unknown profile in the set Ω_l of fig.2, delimited by three half circles whose equations are respectively $\eta^2+\zeta^2=4k^2_{smin}$, $(\eta-k_{smin})^2+\zeta^2=k^2_{smin}$, $(\eta+k_{smin})^2+\zeta^2=k^2_{smin}$, whereas the multimonostatic configuration over the frequency interval $[f_{min},f_{max}]$ allows to retrieve (in the case of a deep probed region) the spectrum of $\Delta\varepsilon_r/z^{0.5}$ in the half annulus Ω_m of fig. 2, that is delimited by the η-axis and by two half-circles whose equations are $\eta^2+\zeta^2=4k^2_{smin}$ and $\eta^2+\zeta^2=4k^2_{smax}$ respectively. Accordingly, the union of the two sets Ω_l and Ω_m coincides with Ω, and so we expect that the classes of retrievable profiles are similar for the two configurations. Moreover Ω_l and Ω_m superpose on each other only for a curve (i.e. a set with a null area), so that the union of the relative data is expected to be not redundant.

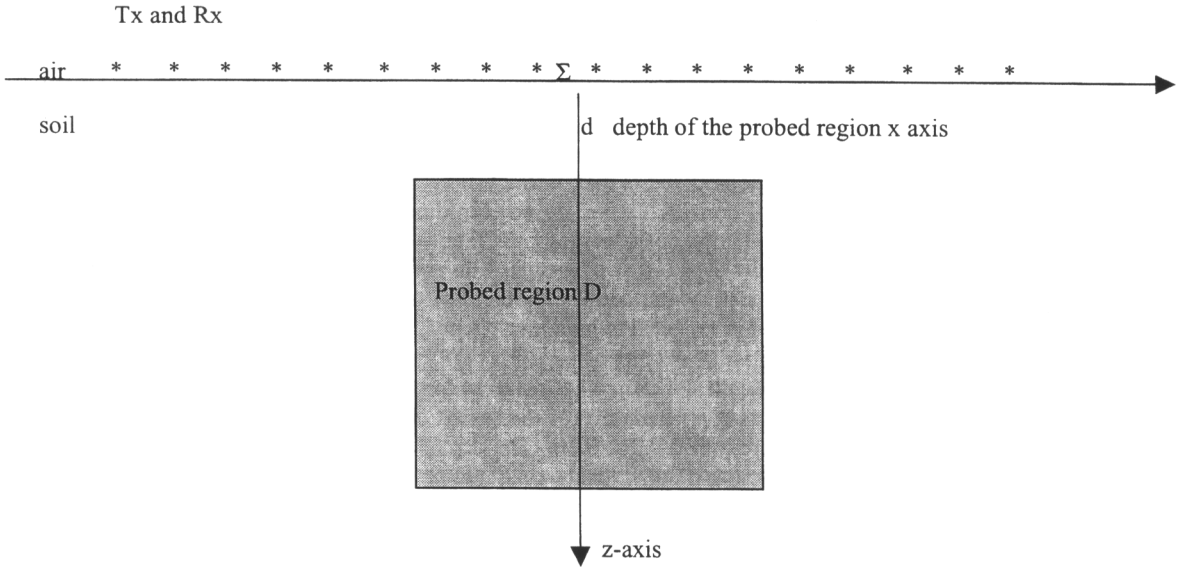

Fig. 1. Geometry of the problem

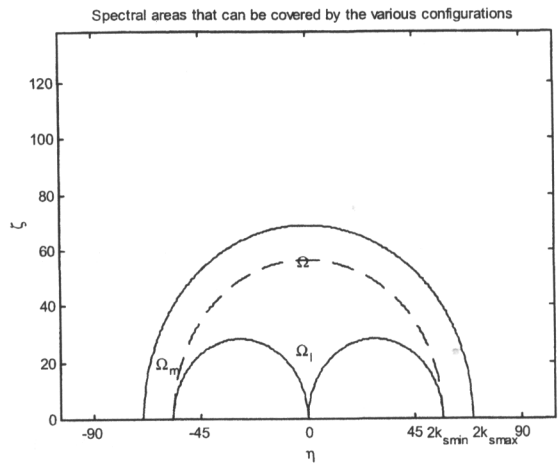

Fig. 2. The outer annulus Ω_m can be "covered" by multimonostatic measurements, the internal set Ω can be covered by multistatic multiview measurements at $f=f_{min}$, the comprehensive set Ω can by covered by the configurations 1 and 2

Actually, it is also to be seen that the spectral coverage exposed is based on rigorous calculations in the case of configuration 1, whereas it is worked out asymptotically in the case of configuration 2 (see Appendixes A and B) when the probed region is deep enough. This "enough", for a three dimensional case, has been quantified of the order of the central adopted wavelength in ref. 13. Moreover, we are aware that to retrieve the spectrum of $\Delta\varepsilon_r/z^{0.5}$ in a certain set does not mean to retrieve the spectrum of $\Delta\varepsilon_r$ in the same set, because an algebraic product in the spatial domain corresponds into a convolution product in the spatial frequency domain. Therefore, apart from the approximations introduced, the two spectral coverages cannot be regarded as theoretically equivalent. Anyway, if the probed region is deep and not greater than the order of the maximum wavelength exploited, we can neglect the variations of the smooth function $1/z^{0.5}$ within the probed region. This suggest two considerations: first, the data collected by varying the frequency of the harmonic incident field and by varying the positions of the transmitting and receiving antennas are not independent on each other (as it has been shown for a one dimensional case in ref. 11) and therefore it is hopeless thickening independently both the number of spatial positions of the antennas and the number of frequencies exploited within a given range. Second, for a given range of frequencies, there exist some information that can be gathered only by varying the positions of the transmitting and receiving antennas: this information concerns low spatial harmonic component of the buried object, and therefore it could be particularly relevant in practical applications, because buried objects are expected to have most of the energy of their spatial spectrum on low spatial frequencies.

3. NUMERICAL EXAMPLES

In this section we expose the numerical results of reconstruction for the two configurations described in the previous section with numerically simulated data. A point to be outlined is that, in the following examples, the reconstruction is based on a finite number of measurements in the spatial domain, i.e. we do not exploit the considerations worked out in the spatial frequency domain in the previous section. Those considerations, in fact, are useful to understand and visualize some expected bounds for the class of retrievable profiles, but any "realistic" inversion have to be founded on a finite number of data. We exploit data simulated under the linear model, because model data are sufficient for our purposes. Moreover, we are going to show cases were the linear model is expected to hold (see e.g. ref. 12 for a quantification). The tool exploited to perform the inversion is a truncated singular value decomposition (TSVD)[20] with threshold 40 dB. The probed region is a square sized 2mx2m, and it begins at the depth d=0.5m. The lower half-space and the objects to be reconstructed are lossless. The relative permittivity of the soil is 9, whereas that of the buried objects is 9.3, so for the case at hand $\Delta\varepsilon_r$=0.3. The objects to be reconstructed are two squares sized 0.2mx0.2m. The depths of the centers of the two objects are equal to 1.1m, they are placed symmetrically with respect to the vertical axis of the probed region, and the distance between the two centers is 0.8m. In order to perform the inversion, the unknown function $\Delta\varepsilon_r$ is expanded in a basis constituted by 20 vertical steps (i.e. 20 Π function of the z-variable) and 21 Fourier harmonics along the x-axis for each step (indexed from –10 up to 10). So the overall number of real unknowns is 840. Measurements are collected at the air-soil interface. The transmitting and receiving antennas are filamentary currents placed along the line Σ, that is centered with respect to the probed region (see fig. 1) and is 5m long. The step between both the transmission and reception positions is 0.15m. The frequency range

exploited is from f_{min}=450MHz up to f_{max}=550 MHz, with a frequency step of 10 MHz. Within the two configurations 1 and 2 the spatial and frequency ranges exploited are the same, as well as the spatial and frequency steps. Fig. 3 shows the behavior of the singular values for the configuration 1, whereas fig. 4 shows the behavior of the singular values for the configuration 2. It can be seen that the singular values "curve" is only a little higher in the case of the configuration 1, in spite of the fact that the number of data exploited has been about 8 times larger (16632 for the configuration 1 and 2194 for the configuration 2). We find interesting to show the behavior of the singular values also in the case of the "simple" multimonostatic configuration, i.e. without adding the multiview multistatic measurements at $f=f_{min}$, and the singular values behavior of the multiview multistatic configuration at $f=f_{min}$ The two behaviors are represented respectively in figs. 5 and 6. It can be seen that the increase in the number of singular values (with reference to the quoted threshold of 40 dB) obtained by adding the two configurations is relevant, and this shows that they provide "quite independent" pieces of information. Let us precise that a similar comparison between the two configurations 1 and 2 is meaningless, because the data of configuration 2 are substantially a proper subset of the data of configuration 1. Fig. 7 shows the reconstruction obtained within configuration 1, while fig. 8 shows the reconstruction obtained within configuration 2. They are comparable, and in both cases the objects are well localized and quantitatively reconstructed. Finally, we find interesting to show also the reconstruction obtained from the simple multimonostatic configuration and from the multiview multistatic configuration at $f=f_{min}$. They are depicted in figs. 9 and 10 respectively. It is worth outlining that the reconstruction of fig. 10 is clearly better than that of fig. 9, in spite of the fact that, for these two configurations, the behavior of the singular values is quite similar. This is a further confirmation of the fact that the class of the retrievable dielectric profiles is different in the two cases (alias, the two configurations provide independent pieces of information). In particular, the multiview multistatic configuration provides information related to low spatial frequencies, that in the case at hand are relevant.

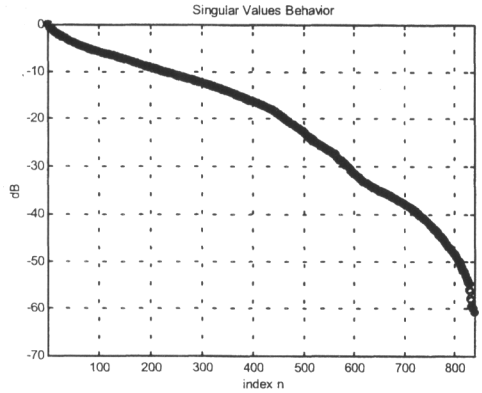

Fig. 3. Singular Values behavior for configuration 1

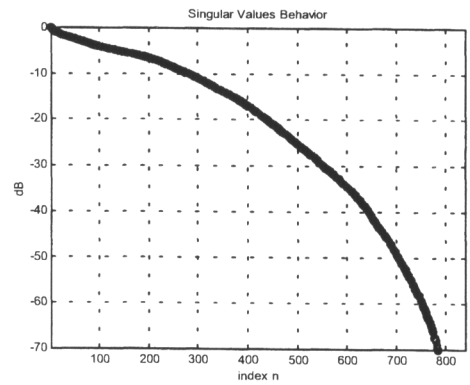

Fig. 4. Singular Values behavior for configuration 2

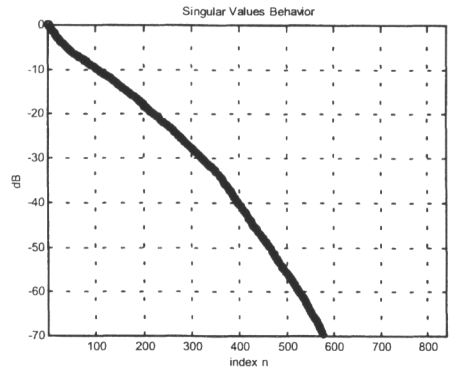

Fig. 5. Singular Values behavior for the multimonostatic configuration

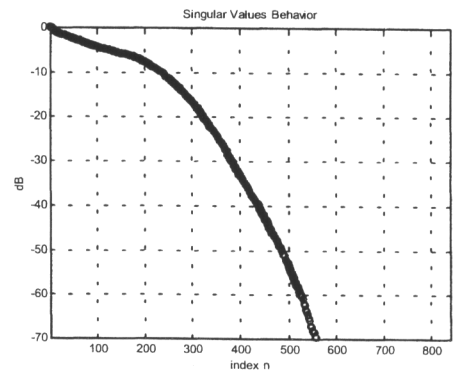

Fig. 6. Singular Values behavior for the multiview multistatic configuration at $f=f_{min}$

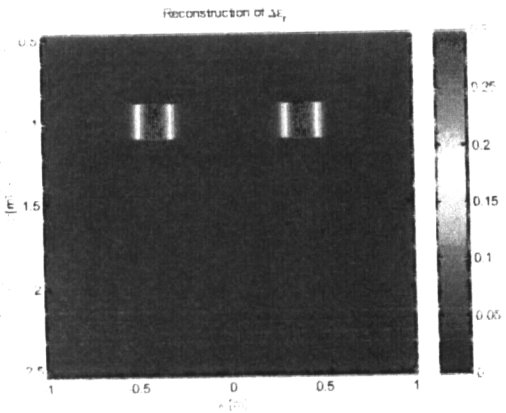

Fig. 7. Reconstruction obtained by configuration 1

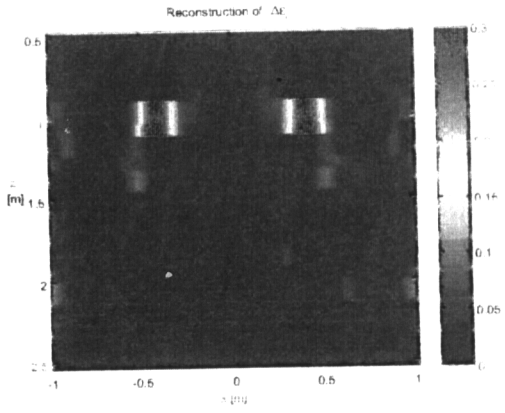

Fig. 8. Reconstruction obtained by configuration 2

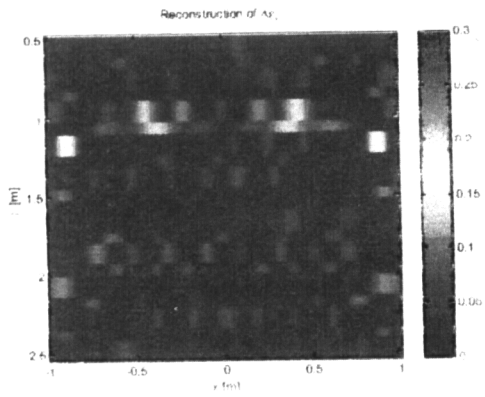

Fig. 9. Reconstruction obtained by the multimonostatic configuration

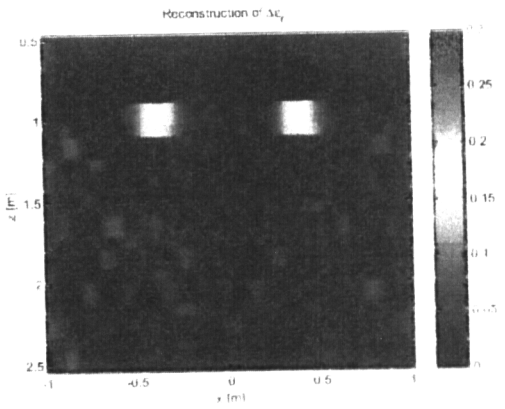

Fig. 10. Reconstruction obtained by the multiview multistatic configuration at $f=f_{min}$

4. CONCLUSIONS

In this work the capabilities of a multistatic multiview scheme for GPR measurements have been investigated. With respect to the more classical multimonostatic scheme, we have shown (in a two dimensional geometry) that multistatic multiview measurements can provide, at a parity of frequency range adopted, valuable information on the low spatial harmonic component of buried objects. Moreover, it has been shown that the set of the locations of the transmitting and receiving antennas and the set of frequencies exploited cannot be regarded as providing independent pieces of information. Actually they are expected to provide non-independent data as far as they allow to retrieve the spectrum of the unknown profile within a same area. The theoretical considerations on which the analysis has been based have been worked out in spectral domains, but the numerical examples shown are inversions in the spatial domain, performed with a finite number of data. The exploitation of multiview and multistatic measurements (at several frequencies) is of relevant interest in GPR applications and it is foreseen within the concrete scientific project ARCHEO. By the end of the current summer, a campaign of measurements will be completed in a controlled site and also in two real archaeological sites in the Southern Italy.

5. ACKNOWLEDGEMENTS

This study has been funded by the Italian Ministry for Universities and Scientific and Technological Research under research contract 179201-1325/458.

6. APPENDIX A

This appendix is devoted to show that a multistatic multiview and multifrequency (over a given frequency range) configuration allows to retrieve the spectrum of the contrast inside the finite set Ω of fig. 2 within the framework of the first order distorted Born approximation. So, let us consider the expression of the scattered field E_s vs. the dielectric profile $\Delta\varepsilon_r$. This expression is well known[7-18]. For a fixed frequency f (time dependence exp(-j2πft) is meant) it is:

$$\mathbf{E}_s = 4\pi^2 f^2 \mu_o \varepsilon_o \iint_D \Delta\varepsilon_r(x',z') Ge(x_o,x',z') \mathbf{E}_{inc}(x',z';x_s) dx'dz' \qquad x_o \in \Sigma \qquad \text{A1}$$

where $Ge(x_o,x',z')$ is the external Green's function of the problem, evaluated at the observation abscissa x_o (let us recall that the measure line is placed at quote z=0). The expression of $Ge(x_o,x',z')$ is

$$G_e(x_o,x',z') = -\frac{j}{2\pi}\int_{-\infty}^{+\infty} \frac{\exp[-jw_s(u)z']}{[w_o(u)+w_s(u)]} \exp[ju(x_o-x')]du \qquad \text{A2}$$

$\mathbf{E}_{inc}(x',z';x_s)$ is the incident field produced in the soil by a current filament directed along the y-axis (see fig. 1) placed at the abscissa x_s (variable on Σ), evaluated in the point (x',z') variable in D. The expression of $\mathbf{E}_{inc}(x',z';x_s)$ is

$$\mathbf{E}_{inc}(x',z';x_s) = -fI_o\mu_o \int_{-\infty}^{+\infty} \frac{\exp[-jw_s(v)z']}{[w_o(v)+w_s(v)]} \exp[jv(x_s-x')]dv \qquad \text{A3}$$

where I_o is the level of the current in the filament. Moreover, ε_o and μ_o are respectively the dielectric permittivity and the magnetic permeability of the vacuum space.

By taking in mind that $\Delta\varepsilon_r$ is assumed equal to zero outside D, and by substitution of eqs. A2 and A3 in eq. A1, it is worked out eq. 2. In eq. 2 it is easy to recognize that the internal integral in dx' and dz' is the Fourier-Laplace transform of the unknown function, evaluated in the points $\eta = u+v$ (as far as the Fourier transform in x') and $\zeta = w_s(u)+w_s(v)$ (as far as the Laplace transform in z'). The outer integral in the variables u and v is, instead, a double inverse Fourier transform evaluated in the points x_o and x_s. Therefore, by considering the double Fourier transform of the scattered field with respect to x_o and x_s, we obtain:

$$\hat{\tilde{E}}_s(u,v) = \frac{j2\pi f I_o \mu_o}{[w_o(v)+w_s(v)][w_o(u)+w_s(u)]} \tilde{\hat{\Delta\varepsilon}}_r(u+v,-j[w_s(u)+w_s(v)]) \qquad \text{A4}$$

where $\hat{\tilde{E}}_s$ is the double Fourier transform of the scattered field and $\tilde{\hat{\Delta\varepsilon}}_r$ is the Fourier–Laplace transform of the unknown function. If we consider only the spectrum of the scattered field for values of |u| and |v| less than k_s, we can replace the Fourier–Laplace transform on the right side of eq. A4 with a double Fourier transform. In fact, in such hypothesis it results:

$$\tilde{\hat{\Delta\varepsilon}}_r(u+v,-j[w_s(u)+w_s(v)]) = \hat{\Delta\varepsilon}_r(u+v,w_s(u)+w_s(v)) \qquad \text{A5}$$

On the other hand, the spectrum of the scattered field is expected to decay outside the square region $|u|,|v| < k_s$ because the Laplace operator, unlike the Fourier operator, contains an exponential attenuation factor in its kernel. Therefore, limiting oneself to consider only the finite region $|u|,|v| < k_s$ of the spectrum of the scattered field is not expected to be critical.

At this point in order to characterize the set in the plane (η,ζ) wherein eq. A4 (with the substitution of eq. A5) allows to retrieve the spectrum of $\Delta\varepsilon_r$, it is needed to study how the set $|u|,|v|< k_s$ is transformed in the plane (η,ζ) by the relationships

$$\begin{aligned}\eta &= u+v \\ \zeta &= w_s(u)+w_s(v)\end{aligned} \qquad \text{A6}$$

This investigation has already been performed[7, 9, 17], and therefore it is known that, e.g. for $k_s = k_{smin}$, the searched set is just the set Ω_1 of fig.2. By increasing in a continuous way f from f_{min} up to f_{max} (which corresponds to increase k_s from k_{smin} up to k_{smax}) the comprehensive area wherein the spectrum of the unknown function can be reliably retrieved clearly corresponds to the set Ω of fig. 2

7. APPENDIX B

In this appendix we show how a multimonostatic configuration for the measurements allows to retrieve the spectrum of the quantity $\Delta\varepsilon_r/z^{0.5}$, under the framework of the first order Born distorted approximation (as already specified), and under the further hypothesis that the probed region is not too shallow (in other words we are going to work out an asymptotic relationship). In order to pursue this end, we consider eq. 2, particularized to the case when $x_o=x_s$:

$$E_s(x_o) = j2\pi f I_o \mu_o \left\{ \frac{1}{4\pi^2} \int_{-\infty}^{+\infty}\int_{-\infty}^{+\infty} \frac{\exp[j(u+v)x_o]}{[w_o(v)+w_s(v)][w_o(u)+w_s(u)]} \times \right.$$
$$\left. \left[\int_0^{+\infty} \exp[-j(w_s(u)+w_s(v))z']dz' \int_{-\infty}^{+\infty} \Delta\varepsilon_r(x',z')\exp(-j(u+v)x')dx' \right] dudv \right\} \qquad \text{B1}$$

By putting $p=u+v \Rightarrow v=p-u$ we have

$$E_s(x_o) = j2\pi f I_o \mu_o \left\{ \frac{1}{4\pi^2} \int_{-\infty}^{+\infty}\int_{-\infty}^{+\infty} \frac{\exp[jpx_o]}{[w_o(p-u)+w_s(p-u)][w_o(u)+w_s(u)]} \times \right.$$
$$\left. \left[\int_0^{+\infty} \exp[-j(w_s(u)+w_s(p-u))z']dz' \int_{-\infty}^{+\infty} \Delta\varepsilon_r(x',z')\exp(-jpx')dx' \right] dudp \right\} \qquad \text{B2}$$

Also in this case, it is easy to recognize an inverse Fourier transform calculated in x_o and a Fourier transform with respect to the variable x'. By considering the Fourier transform of the scattered field, it is so possible to work out (by making use of the same symbols adopted in appendix A) the following relationship:

$$\hat{E}_s(p) = jfI_o\mu_o \int_{-\infty}^{+\infty}\int_{-\infty}^{+\infty} \frac{\hat{\Delta\varepsilon}_r(p,z')\exp[-j(w_s(u)+w_s(p-u))z']}{[w_o(p-u)+w_s(p-u)][w_o(u)+w_s(u)]} dudz' \qquad \text{B3}$$

At this point, if the probed region is deep "enough", the integral in the variable u can be evaluated with the approximate procedure of the stationary phase, exploited (e.g.) in ref. 13 in a three dimensional case.

Therefore, we obtain

$$\hat{E}_s(p) \cong \frac{jfI_o\mu_o \exp\left(-j\frac{\pi}{4}\right)}{[w_o(\frac{p}{2})+w_s(\frac{p}{2})]^2} \sqrt{\frac{\pi\left(w_s(\frac{p}{2})\right)^3}{2\left(\left(w_s(\frac{p}{2})\right)^2+\left(\frac{p}{2}\right)^2\right)}} \int_{-\infty}^{+\infty} \hat{\Delta\varepsilon}_r(p,z')\exp[-j2w_s(\frac{p}{2})z']\frac{1}{\sqrt{z'}}dz' \qquad \text{B4}$$

The integral at second member of eq. B4 is by definition the double Fourier transform of $\Delta\varepsilon_r/z^{0.5}$ evaluated in the points $\eta = p$ (conjugate of the horizontal spatial variable) and $\zeta = 2w_s(\frac{p}{2})$ (conjugate of the depth), as far as $w_s(\frac{p}{2})$ is real (incidentally, if $w_s(\frac{p}{2})$ is not real the approximation on which the stationary phase procedure is based does not hold). This means that we limit ourselves to consider the spectrum of the scattered field only within the interval $[-2k_s, 2k_s]$. Again, this is not expected to be a severe limitation because, if $|p|>2k_s$, at least one of the two quantities $w_s(u)$ or $w_s(p-u)$ provides an exponentially attenuating factor in eq. B3.

Therefore, the point is now to analyze which curve is described on the plane (η,ζ) when p spaces from $-2k_s$ up to $2k_s$.

The transformation to be considered is:

$$\eta = p$$
$$\zeta = 2w_s(\frac{p}{2}) \qquad \text{B5}$$

It is easy to verify that the curve obtained on the plane (η,ζ) is a half circle having center in the origin of the axes and having radius equal to $2k_s$. Therefore, by increasing in a continuous way f from f_{min} up to f_{max} (which corresponds to increase k_s from k_{smin} up to k_{smax}) the comprehensive area wherein the spectrum of $\Delta\varepsilon_r/z^{0.5}$ can be reliably retrieved corresponds to the half annulus Ω_m of fig. 2. Finally, since (from Appendix A) multistatic multiview measurements at $f=f_{min}$ allow to "cover" the set Ω_1 of fig. 2, comprehensively configuration 2 allows to cover the same spectral area Ω covered by configuration 1.

REFERENCES

1 D. J. Daniels, "Surface-penetrating Radar, The Institution of Electrical Engineers (London, 1996)

2 G. R: Olhoeft, "Application of Ground Penetrating Radar", in Proc. of the 6th Int. Conf. On Ground-Penetrating Radar, Senday, JAPAN, 1996.

3 L. A. Robinson, W. B. Weir, and L. Young, " Location and Recognition of Discontinuities in Dielectric Media Using Synthetic RF Pulses, Proc. of IEEE, vol. 62, n. 1, pp 36-44, January 1974.

4 D. A. Noon, " Stepped-Frequency Radar Design and Signal Processing Enhances Ground Penetrating Radar Performance, Ph.D. thesis, Deparment of Electrical & Computer Engineering, The University of Queensland and Cooperative Research Centre fir Sensor Signal and Information Processing, January 1996.

5 G. F. Stickley, D. A. Noon, M. Cherniakov, I.D. Longstaff, "Gated stepped-frequency ground penetrating radar", Journal of Applied Geophysics, vol. 43, n. 2000, pp. 259-269, march 1999

6 S. K. Koppenjan, C. M. Allen, D. Gardner, H. R. Wong, H. Lee, and S. J. Lockwood, "Multi-frequency synthetic-aperture imaging with a lightweight ground penetrating radar system, vol. 43, n. 2000, pp. 251-258, October 1999.

7 D. Lesselier, B. Duchene, "Wavefield inversion of objects in stratified environments: from back-propagation schemes to full souìlutions", in Review of Radio Science 1993-1996, ed. R. Stone, Oxford University press, 1996.

8 R. Pierri, G. Leone, "Nonlinear models in inversion algorithms for tomographic reconstructions" in Proc. of the 8th Int. Conf. On Ground-Penetrating Radar, Queensland, Australia, 2000.

9 R. Pierri, G. Leone and R. Persico, "Quadratic models in inverse scattering: numerical experiments" in Proc. of International Geoscience And Remote Sensing Symposium, Hamburg (Germany) June 1999.

10 W.C.Chew, Waves and fields in inhomogeneous media, IEEE Press, 1995.